3D printing of inorganic scintillator-based particle detectors

T. Sibilieva,[a,*] **V. Alekseev,**[a] **S. Barsuk,**[b] **S. Berns,**[c,d,e] **E. Boillat,**[c,d,e] **I. Boiaryntseva,**[a,b]
A. Boyarintsev,[a] **A. Carbone,**[f,i] **A. De Roeck,**[g] **S. Dolan,**[g] **T. Driuk,**[a] **A. Gendotti,**[h]
I. Gerasymov,[a] **B. Grynyov,**[a] **S. Hugon,**[c,d,e] **U. Kose,**[h] **O. Opolonin,**[a] **A. Rubbia,**[h]
D. Sgalaberna,[h] **M. Sibilyev,**[a] **S. Tretyak,**[a] **T. Weber,**[h] **J. Wuthrich**[h] and **X.Y. Zhao**[h]

[a]*Institute for scintillation materials National Academy of Science of Ukraine (ISMA NAS of Ukraine),*
Nauki ave. 60, Kharkiv 61072, Ukraine

[b]*Laboratoire de Physique des 2 Infinis, Iréne Joliot-Curie, Universitè Paris-Saclay,*
Universitè de Paris, IN2P3/CNRS, 91405 Orsay, France

[c]*Haute Ecole Spécialisée de Suisse Occidentale (HES-SO),*
CH-2800 Delémont, Route de Moutier 14, Switzerland

[d]*Haute Ecole d'Ingénierie du canton de Vaud (HEIG-VD),*
CH-1401 Yverdon-les-Bains, Route de Cheseaux 1, Switzerland

[e]*COMATEC-AddiPole, CH-1450 Sainte-Croix, Technopole de Sainte-Croix,*
Rue du Progrès 31, Switzerland

[f]*Istituto Nazionale Di Fisica Nucleare (INFN), Sezione di Bologna,*
Viale C. Berti Pichat, 6/2, 40127, Bologna, Italy

[g]*Experimental Physics department, European Organization for Nuclear Research (CERN),*
Esplanade des Particules 1, 1211 Geneva 23, Switzerland

[h]*Institute for Particle physics and Astrophysics, ETH Zurich,*
Otto-Stern-Weg 5, CH-8093 Zurich, Switzerland

[i]*Università di Bologna,*
Via Zamboni, 33, 40126 Bologna, Italy

E-mail: sibilieva@isma.kharkov.ua

ABSTRACT: Inorganic scintillators are widely used for scientific, industrial and medical applications. The development of 3D printing with inorganic scintillators would allow the fast creation of detector prototypes for the registration of ionizing radiation, such as alpha, beta and gamma particles in thin layers of active material, and X-ray radiation. This article reports on the technical work and scientific achievements that aimed at developing a new inorganic scintillation filament to be used for the 3D printing of composite scintillator materials: study and definition of the scintillator composition; development of the methods for the inorganic scintillator filament production and further implementation in the available 3D printing technologies; study of the impact of the different

---

*Corresponding author.

3D printing modes on the material scintillation characteristics. Also, 3D-printed scintillators can be used to produce combined detectors for high-energy physics.

Contents

1 Introduction

In the last years, more and more attention has been paid to additive manufacturing technologies (AM), also called 3D printing, to obtain functional materials in modern material science. The improvement in the available AM technologies is accompanied by a significant reduction of the costs, which makes 3D printing a viable solution not only for fast prototyping but also for the final production of finite objects.

The 3D printed Detector (3DET) R&D collaboration [1] aims at developing 3D printing for scintillator-based particle detectors. For instance, the 3DET collaboration aims to 3D print the active scintillator part and the other detector components, such as the dark box, optical connectors, etc. As we have shown recently, plastic scintillators based on polystyrene were manufactured using fused deposition modeling (FDM) 3D printing technology with characteristics comparable with the standard production techniques such as cast polymerization, extrusion, and injection molding [2]. Moreover, FDM technology allows printing of both scintillator and reflector at once by using two extruders [3]. Hence, it allows to create multi-element scintillation detectors, such as an array of scintillation cubes or tiles separated by a reflector, as well as the production of combined scintillation detectors from several scintillation materials.

Although the results obtained in [3] are very promising, work is in progress in order to improve the 3D printed scintillator performance, the geometrical tolerance and the uniformity in the reproducibility of multiple samples, towards the first real particle detector ever 3D printed. The main goal will be the fast and cost-effective production of massive fine-granularity polystyrene-based plastic-scintillator detectors with applications in high-energy physics (HEP), such as neutrino active

scintillator targets or particle calorimetry [4]. However, AM also shows a strong potential for applications beyond HEP.

A large number of scintillation materials and detectors for high energy physics are known. In addition to plastic scintillators, inorganic scintillators are widely used for radiation detection, such as $Gd_3Al_2Ga_3O_{12}$:Ce (GAGG:Ce), Y_2SiO_5:Ce (YSO:Ce), $Y_3Al_5O_{12}$:Ce (YAG:Ce), $Lu_3Al_5O_{12}$:Ce (LuAG:Ce), Gd_2O_2S:Pr (GOS:Pr), ZnSe:Al, CsI:Tl, etc. [5–8].

The development of 3D printing with inorganic scintillators would allow to create fast prototypes of detectors for the registration of charged particles, such as alpha, beta and gamma particles in thin layers of active material, and X-ray radiation. For 3D printing using FDM technology, a thermoplastic filament is required as a starting material. The production of such a filament for printing scintillators is possible if a composition is created from granules of inorganic scintillators and transparent thermoplastic polymers. The implementation of 3D printing in the manufacturing of composite inorganic scintillators makes the creation of scintillators with the required geometry possible without additional machining. In fact, all 3D printed samples presented in this work were not subjected to either grinding or polishing.

Previously [9–13], we investigated composite scintillators based on grains of inorganic single crystals. Polysiloxane elastomer was used as a binder. Single crystals were mechanically ground up to obtain scintillation grains. After that, a set of calibrated sieves was used to select the fraction of grains with the optimal size. Then, the grains were introduced in the liquid polysiloxane with pre-added polymerization catalyst and the composition was mixed. Finally, the composition was introduced into a forming container, in which it was left to complete its polymerization. As a result, the scintillator is obtained and can be taken from the forming container. Composite scintillators with inorganic single crystals are a promising alternative to bulk inorganic scintillation detectors. In particular, to make large area detectors at a reasonable price thanks to the possibility of using the waste from the production of single crystals.

This article reports on the technical work and scientific achievements that aimed at developing a new inorganic scintillation filament to be used for the 3D printing of composite scintillator materials: study and definition of the scintillator composition; development of the methods for the inorganic scintillator filament production and further implementation in the available 3D printing technologies; study of impact of the different 3D printing modes on the material scintillation characteristics. In the following sections, we will discuss the results of the latest R&D.

2 Obtaining scintillation filaments with inorganic granules and 3D printing of scintillators

In this work, inorganic scintillator-based 3D printed samples from ZnSe:Al, GOS:Pr, GAGG:Ce and CsI:Tl were obtained and tested. Such inorganic scintillators are widely used in radiography and X-ray computed tomography from medical to industrial applications due to their high efficiency X-ray absorption and high light output. For instance, the samples of 1 mm thickness are efficient for registration of X-rays with energies of a few tens of keV.

The scintillator filaments were made on the basis of the above-mentioned inorganic scintillators with the addition of polymeric materials as an optical binder. PS (polystyrene), ABS (acrylonitrile

butadiene styrene), SBS (styrene-butadiene-styrene) and PMMA (polymethyl methacrylate) polymer pellets were chosen as optical binders due to their high transparency to visible light.

The use of inorganic scintillation granules as part of filament compositions significantly expands the possibilities of using 3D printing technology also for inorganic scintillators. The material for 3D printing with FDM technology is a thermoplastic filament, produced by mixing inorganic granules with polymer pellets.

Figure 1. Left: planetary mill Fritsch Pulverisette 5/2; right: set of sieves for fractioning of the inorganic scintillation granules.

The first stage consists of the grinding of scintillation inorganic crystals. As shown in figure 1, the planetary mill Fritsch Pulverisette 5/2 [14] was used for grinding and producing inorganic scintillation granules. An appropriate set of sieves was used to select the inorganic scintillation granules of the required size: 1–15, 45–63, 63–100, and 100–140 µm.
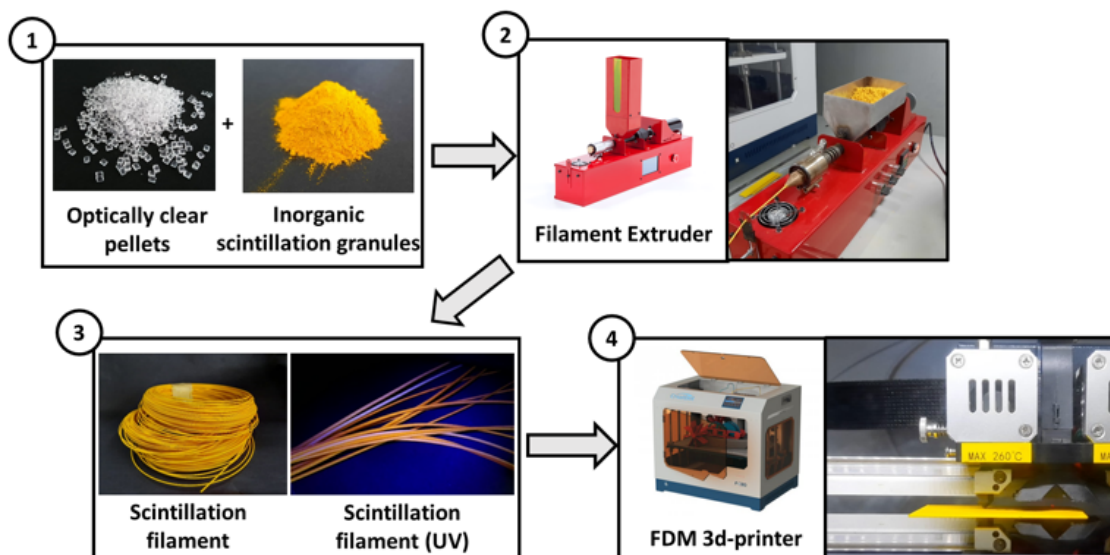

Figure 2. The process of production of filament with inorganic scintillation granules and 3D printing of the scintillator.

The next step is the production of scintillation filament for 3D printing. As shown in figure 2, its production consists of the following steps:

- plasticizer and scintillation inorganic granules were added to the optically-transparent polymer pellets (binder) and mixed;

- the resulting mixture was loaded into a Noztek ProHT extruder [15] to form the filament; the diameter of the obtained filament was controlled by an electronic caliper;

- finally, a scintillating filament with a diameter of 1.75 ± 0.05 mm was produced.

The optimal temperature regimes for obtaining the scintillation filaments with the addition of inorganic granules is shown in table 1.

Table 1. Temperature regimes for obtaining scintillation filaments depending on the type of polymer pellets (binder).

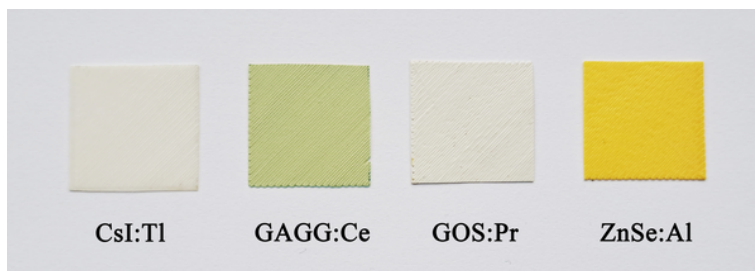| Type of polymer	Optimal printing temperature, °C
PS	200–235
PMMA	250–270
ABS	220–250
SBS	210–230

Figure 3. 3D printed samples $20 \times 20 \times 1$ mm with inorganic scintillation granules CsI:Tl, GAGG:Ce, GOS:Pr, ZnSe:Al with PS as an optical binder.

Scintillation filaments based on ZnSe:Al, GOS:Pr, GAGG:Ce and CsI:Tl granules for 3D printing using FDM technology have been developed. The FDM Creatbot F430 printer [16] was used to obtain 3D printed samples. SolidWorks 3D CAD software was used to design 3D scintillator sample model. CreateWare was used as a slicer to break up the designed model into layers for 3D printing. The printing bed and nozzle temperature as well as the printing speed and other parameters were set depending on the type of filament. As we discovered earlier [2], increasing the temperature of the chamber, bed, and extruder improves the scintillator transparency. The samples in this work were printed at the maximum printing temperature for each type of polymer pellets, see table 1. The bed temperature at printing was 110 degrees, which is the maximum temperature that the printer can handle. The printing speed was between 25 mm/s to 35 mm/s, with a layer thickness between 0.1 to 0.2 mm. Figure 3 shows 3D printed samples with the different inorganic scintillation granules.

3 Properties of the 3D printed inorganic scintillators

3.1 Research methodology

Measurements of decay times were carried out by using a combined fluorescent lifetime and steady-state spectrometer FLS 920 (Edinburgh Instruments) equipped with a hydrogen filled nF 900 ns flashlamp with an optical pulse duration of 1.0–1.6 ns and pulse repetition rate of 40 kHz, for time correlated single photon counting measurements. The X-ray tube and the photodetector Hamamatsu R1926A were placed on the same side from the samples. X-ray luminescence spectra were measured in the reflection mode under a steady-state X-ray excitation by applying voltage of 40 kV and current of 40 µA on Ag anode. The emitted light was dispersed with a monochromator with grating 1200 grooves/mm. The obtained spectra were not corrected for the spectral sensitivity of the detection system.

Measurements of the X-ray relative light output of the 3D printed scintillators were carried out on the stand by measuring and comparing the light output of different scintillators [17]. The samples were irradiated with X-rays at a source anode voltage of 90 kV. The radiation beam was limited by a lead collimator 3 mm in diameter. The light output of the objects under the test was compared with the reference — a ZnSe:Al single crystal $20 \times 20 \times 1$ mm in size. The scanning step was determined to be 5×5 mm. For one measuring process a reference sample and five 3D-printed samples were located into the stand. With the selected scanning parameters, 16 measurement points on the samples can be obtained. The measurement results were recorded in arbitrary units (values of the ADC stand). After averaging the values for each sample, the light output of each sample relative to the reference was calculated using a proportional transformation. For example, the signal of the reference sample is 987 and the signal of the 3D-printed sample is 546, then the relative light output of the 3D-printed sample equals $100\% \cdot 546/987 = 55.32\%$. The scintillation light output efficiency spectra were measured with the Hamamatsu R1307 PMT by exciting with alpha particles from Pu-239 source and beta particles from Bi-207 source. A signal from PMT anode was fed into Rigol DS1302CA oscilloscope.

The spatial resolution of 3D printed scintillators was determined using a self-made X-ray imaging setup [18] with the following characteristics: Isovolt Titan E 160 X-ray source with W anode; inherent filtration (mm) 0.8/Be; max. Ua = 160 kV, Ia = 10 mA; nom. focal spot value IEC 336 — 1.5 (0.4); focal spot size EN 12 543 (mm) — 3(1). Spatial resolution was determined on images taken with a digital photocamera by checking the quantity of resolved wire pairs using an EN 462-5 Duplex IQ standard containing 13 pairs of wires with the different diameters. The images were captured by a Canon camera with the 3264×2448 (8 megapixels) resolution. Distance from the X-ray source to the composite scintillator was around 0.5 m. All the measurements were performed at room temperature.

3.2 Studying luminescence and decay time of the samples

The X-ray luminescence and decay time results were compared with the inorganic scintillation granules obtained in section 2 (see figure 1). The results of the study of luminescence and decay time of the 3D printed samples are shown at figures 4 and 5. The scintillation properties of the 3D printed samples are similar to inorganic scintillator granules. The size of the 3D printed samples was $20 \times 20 \times 1$ mm, as an optical binder of the samples was used PS. A sample of pure PS of the same

size was also 3D printed and its transmittance was measured. As shown in figure 6 the transmittance of the pure PS is about 90–93% in 350–800 nm range, thereby it should not affect the luminescence spectrum of scintillation material. Inorganic scintillator granules for measurement were placed in $\varnothing 10 \times 2$ mm cuvettes.
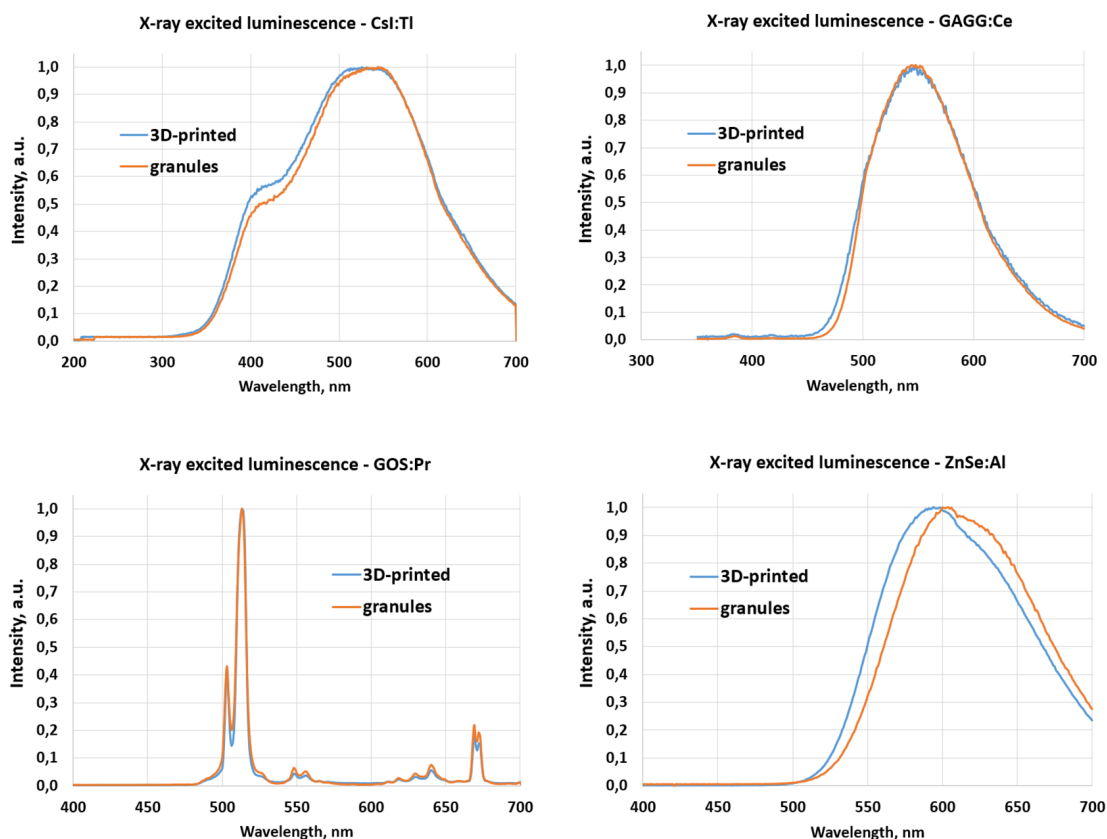

Figure 4. X-ray luminescence spectra of 3D printed samples and inorganic scintillation granules CsI:Tl, GAGG:Ce, GOS:Pr, ZnSe:Al with PS as an optical binder.

The measurement results are quantitatively displayed in table 2. 3D printing, as well as the binder (PS), does not lead to changes in the X-ray luminescence spectra and does not affect the decay time.

3.3 X-ray registration: dependence of light output on particle size distribution, granules concentration and thickness, X-ray light output uniformity

The samples of 3D printed scintillators with 25-75% weight content of ZnSe:Al for X-ray registration were prepared as shown in figure 7. Several thicknesses from 0.2 mm to 1.2 mm and granules size in the ranges 1–15, 45–63, 63–100 and 100–140 μm were tested.

As a reference for the measurement, we used a ZnSe:Al single crystal with a size of 20×20×1 mm as shown in figure 8. The samples were photographed under the day light. The observed difference in the color is due to the different light reflection/absorption conditions for the single crystal and 3D printed scintillator with ZnSe:Al granules. For granules the diffused reflection predominates over
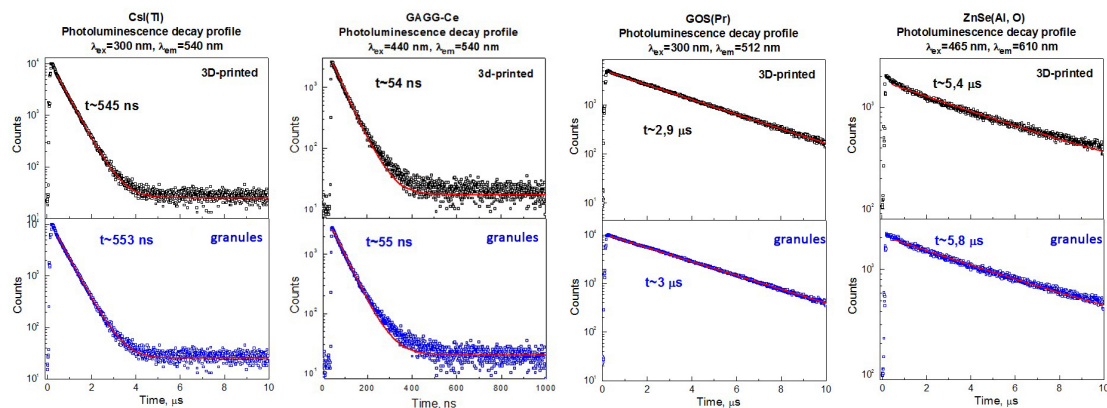
Figure 5. Photoluminescence decay profiles of 3D printed samples and inorganic scintillation granules CsI:Tl, GAGG:Ce, GOS:Pr, ZnSe:Al with PS as an optical binder.
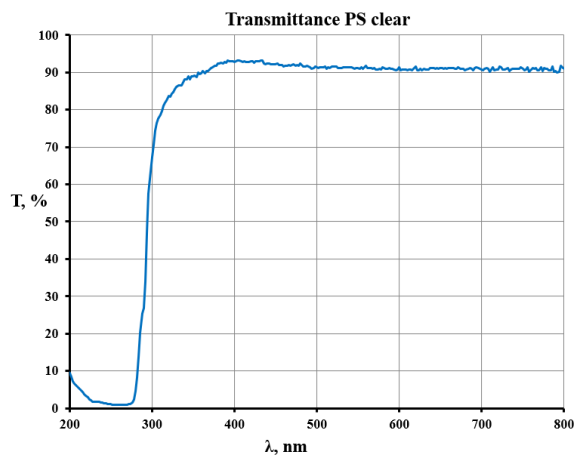

Figure 6. Transmittance of the pure PS.

Table 2. Positions of X-ray luminescence maxima and decay constants values under photo excitation for inorganic scintillation granules and 3D printed samples with PS as an optical binder.

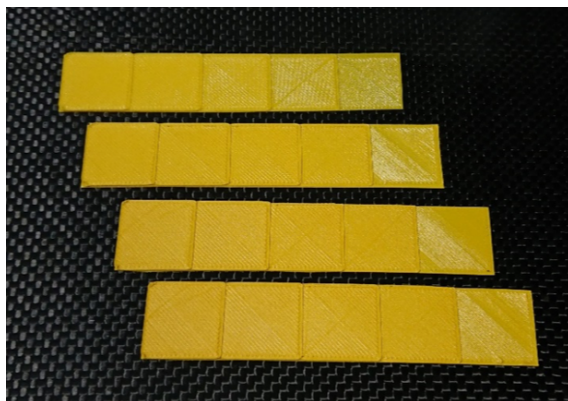| Scintillator	Type of scintillator	Position of X-ray luminescence maximum λ_{max}, [nm]	Decay time [ns]	Error [ns]
Cs:Tl	Inorganic granules	540	553	0.57
	3D-printed sample	540	545	0.70
GAGG:Ce	Inorganic granules	547	55	0.14
	3D-printed sample	547	54	0.14
GOS:Pr	Inorganic granules	512	3000	3.24
	3D-printed sample	512	2900	3.59
ZnSe:Al	Inorganic granules	610	5800	19.88
	3D-printed sample	610	5400	22.74

Figure 7. 3D printed scintillators with ZnSe:Al granules.

Figure 8. Left: ZnSe:Al single crystal. Right: 3D printed scintillator with ZnSe:Al granules.

the absorption since granules have a rough uneven surface. That is why the granules demonstrate less coloration. (The same effect can be observed if one milled the green glass — the glass powder will have almost white color instead of green due to high diffused reflection).

The dependence of the light output on the concentration of the inorganic scintillator granules is shown in figure 9. The concentration of the inorganic granules in the filament is shown on the X axis while the light output is given on the Y axis. Samples of various thicknesses, from 0.2 to 1.2 mm, were tested and compared to the industrial scintillator sample.

The optimal weight content of inorganic granules in the scintillation filament (with respect to light output and mechanical characteristics for using in 3D printer) is obtained to be 50–60%. Printing filament with the granules weight content more than 60% is difficult, as the filament crumbles. Printing filament with a granule weight content less than 50% leads to the light output decrease, thus a lower particle registration efficiency. The dependence of the light output on the sample thickness is shown in figure 10. The optimal sample thickness is obtained to be 0.8–1.0 mm.

To study the uniformity of the distribution of inorganic granules inside the filament, a sample of $60 \times 100 \times 0.3$ mm was printed. A filament with ZnSe:Al granules 63–100 μm in size and 30% weight content was used for printing. The X-ray light output uniformity of this was studied. As a reference was used a ZnSe:Al single crystal with a size of $20 \times 20 \times 0.3$ mm, which was located near the 3D-printed sample for measuring. The visualization of the signals obtained on this sample is shown in figure 11-a. The non-uniformity of the light output of the sample was defined to be the ratio of signals: (maximum-minimum)/ average, is determined to be 46%. However, the visualization of the signal
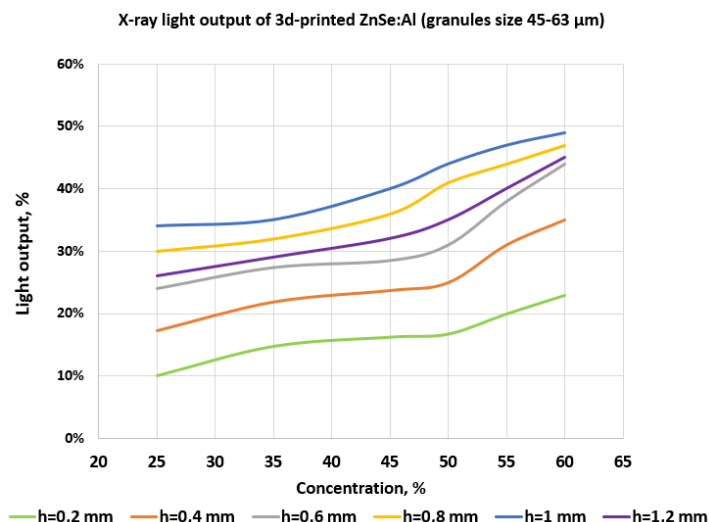
X-ray light output of 3d-printed ZnSe:Al (granules size 45-63 µm)

Light output, %

— h=0,2 mm   — h=0,4 mm   — h=0,6 mm   — h=0,8 mm   — h=1 mm   — h=1,2 mm

Figure 9. X-ray light output of 3D printed scintillators with different concentration of ZnSe:Al granules relative to the single crystal ZnSe:Al. Different sample thicknesses (h) were tested (granules size was 45–63 micrometers).
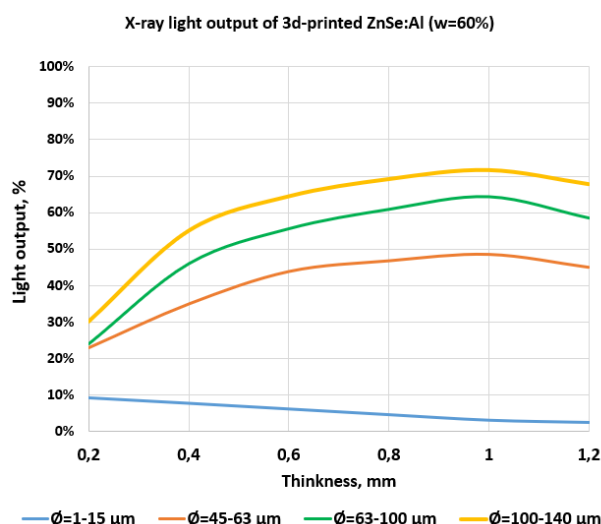
X-ray light output of 3d-printed ZnSe:Al (w=60%)

Light output, %

Thinkness, mm

— Ø=1-15 µm   — Ø=45-63 µm   — Ø=63-100 µm   — Ø=100-140 µm

Figure 10. X-ray light output of 3D printed scintillators with different thickness relative to the single crystal ZnSe:Al $20\times20\times1$ mm. Different granules size ($\varnothing$) were tested (weight content of inorganic granules was 60%).

shows that such a high nonuniformity is associated with the direction of the nozzle stroke. Therefore, it was decided to change the direction of the nozzle stroke. To do this, in the CreatWare program, the position of the sample on the stage was shifted by 45 degrees. Thus, instead of the diagonal direction of the nozzle stroke, we got a parallel one. In this way, a second sample of the same size was printed using the same filament. The visualization of the signals obtained on the second sample is shown in figure 11-b. The non-uniformity of the second sample was 15%, which is probably due to the non-uniformity of the distribution and segregation of inorganic granules inside the filament.
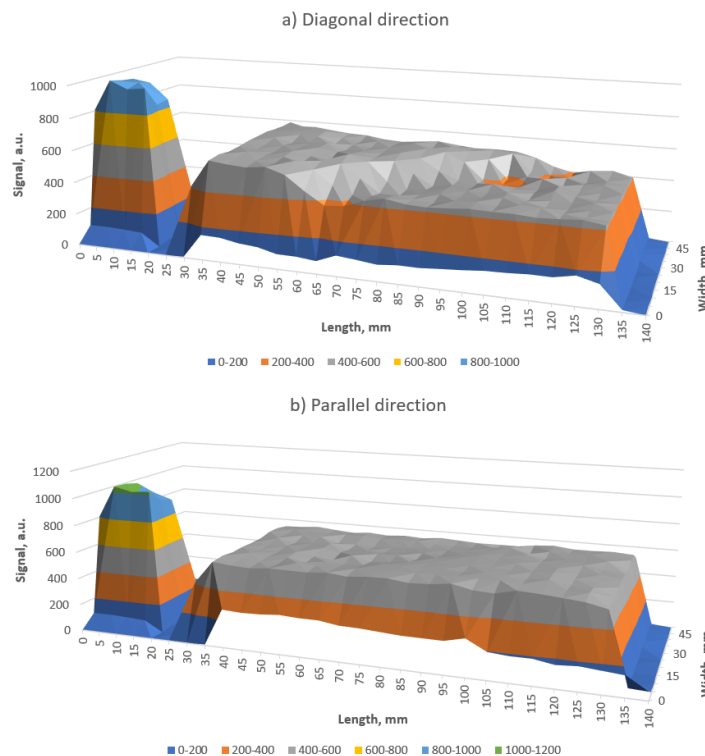
Figure 11. X-ray light output uniformity: a) sample with the diagonal direction of the nozzle stroke; b) sample with the parallel direction of the nozzle stroke.

3.4 Registration of alpha- and beta-radiation: dependence of light output on polymers as an optical binder

Two inorganic scintillators with ZnSe:Al and ZnS:Ag were 3D printed for the detection of alpha particles. The size of the inorganic granules was 40–63 µm, and the size of 3D printed samples was $\varnothing 44 \times 0.2$ mm. The samples based on ZnSe:Al granules were printed with PS, ABS, SBS, and PMMA polymers as optical binder. The samples based on ZnS:Ag granules were printed only with PS polymers as an optical binder. As a reference, the $\varnothing 44 \times 1$ mm ZnSe:Al single crystal produced by ISMA [20] was used. Both the 3D printed samples and ZnSe:Al single crystal were coupled to $\varnothing 44 \times 8$ mm PMMA light guide (see figure 12) for a better light collection. The side surface of the light guides is wrapped in two layers of a PTFE membrane. Also, as references $\varnothing 44$ mm Alpha Detector ZnSe based by ISMA [20] was used, this sample already contains $\varnothing 44 \times 8$ mm PMMA light guide in its design. The samples are shown in figure 12.

Each sample was exposed with a Pu-239 source up to a set of 100 thousand events. The light output was determined from the maximum of the amplitude spectrum. Among various polymers, the best results were obtained with PS and PMMA as an optical binder (see table 3). Their light output reaches 94% compared to ZnSe:Al single crystal. However, it should be noted that the counting rate of these 3D printed samples was 2.5 times lower compared to the single crystal. The counting rate was determined as the ratio of the number of events to the exposure time. This means that it took 2.5 times longer to set 100 thousand events for a 3D-printed sample. The decrease in the

Figure 12. PMMA light guide and samples for alpha particle registration.

Table 3. Relative light output of 3D printed ZnSe:Al and ZnS:Ag based scintillators with different plastics as an optical binder under Pu-239 source (weight content of inorganic granules was 50%)

Sample	Relative light output, %	Counting rate, %
ZnSe:Al single crystal	100	100
Alpha Detector ZnSe based	127	200
3D printed ZnS:Ag with PS	180	100
3D printed ZnSe:Al with PS	94	40
3D printed ZnSe:Al with PMMA	94	40
3D printed ZnSe:Al with ABS	66	20
3D printed ZnSe:Al with SBS	39	10

counting rate may be related to a decrease in the probability of interaction of alpha particles with a scintillation material, since some of the alpha particles will be absorbed by the optical binder without light emission. It also can be due to the absorption and scattering of light in the volume of the 3D printed scintillator.

The ZnS:Ag 3D printed sample shows a very good result, its relative light output is 180% and the counting rate is 100% compared to ZnSe:Al single crystal. Spectra of registration of alpha-radiation from Pu-239 are shown in figure 13.

Table 4. Relative light output of 3D printed ZnSe:Al based scintillator with PS as an optical binder under Bi-207 source (weigh content of inorganic granules was 50%)

Sample	Relative light output, %	Counting rate, %
ZnSe:Al single crystal	100	100
3D printed ZnSe:Al with PS	98	40

3D printed sample with size $20 \times 20 \times 1$ mm was printed for detection of beta-particles. The size of ZnSe:Al granules was 100–300 μm. 3D printed samples with a granules size of < 100 μm turned out to be insensitive to beta-radiation. Producing a filament and 3D printing with granules > 300 μm is difficult due to the rapid wear of extruder parts, as well as nozzles and feed rollers of the 3D printer. Therefore, the granule size of 100–300 μm is optimal for 3D printing of samples sensitive to beta-radiation. As a reference, $20 \times 20 \times 1$ mm ZnSe:Al single crystal was used. For beta-irradiation, the light output was determined from the position of the maximum of the total absorption peak of conversion electrons with energy of 976 keV. The light output of the 3D printed
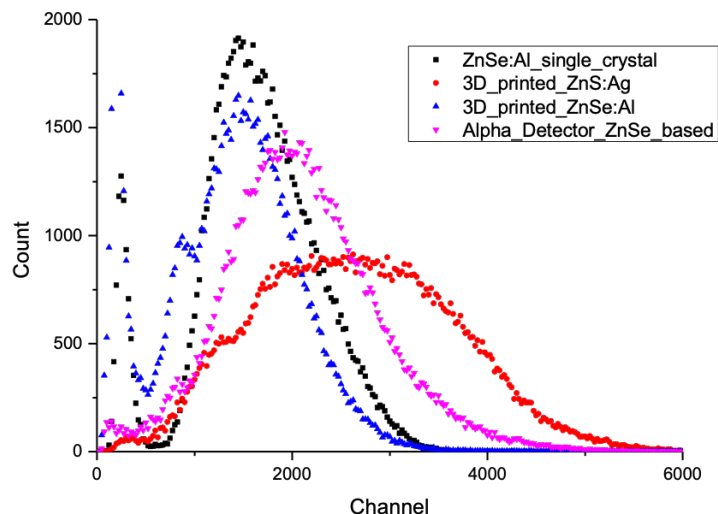
Figure 13. Spectra of registration of alpha-radiation (Pu-239) of ZnSe:Al and ZnS:Ag 3D printed samples with PS as an optical binder, ZnSe:Al single crystal and Alpha Detector ZnSe based.

sample was 98% compared to the single crystal. But as in the case of irradiation with alpha-particles, the counting rate of the printed sample was also 2.5 times lower than that of the single crystal (see table 4). The spectra of the registration of beta-radiation (Bi-207) are shown in figure 14.
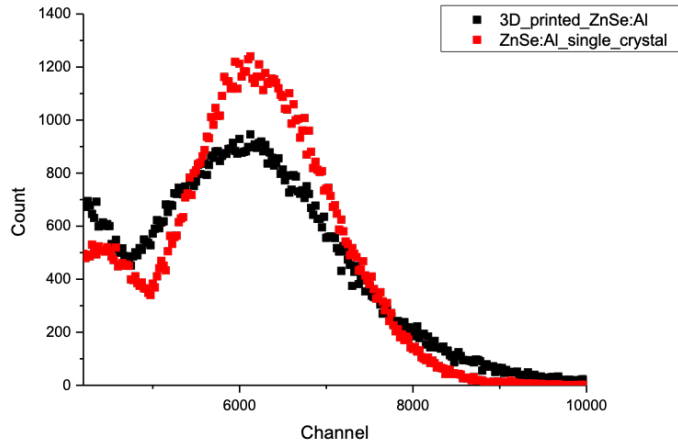

Figure 14. Spectra of registration of beta-radiation (Bi-207) of ZnSe:Al 3D printed sample with PS as an optical binder and ZnSe:Al single crystal

3D printing allows the printing of both organic and inorganic scintillators for simultaneous alpha- and beta- registration. There can be prospects for combining organic and inorganic scintillators in a detector with increased registration sensitivity. We have printed the first prototype of the combined detector, which is shown in figure 15. Combinations of different scintillators result in achieving unique effects and this will be the subject of further research.
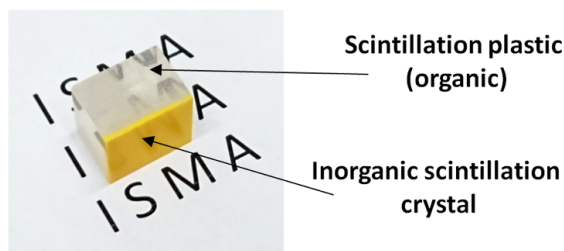
Figure 15. First 3D printed prototype of the combined detector after post-processing.

3.5 X-ray imaging

Films for X-ray imaging, effective for registration of soft X-ray radiation (20–90 keV), were obtained on the basis of ZnSe:Al, GOS:Pr, GAGG:Ce and CsI:Tl granules (see figure 16). The size of granules was 1–15 µm. Composite filaments were fabricated with 60% by weight of scintillation granules using PS as an optical binder. Composite films were obtained with a thickness of 0.15 mm to 0.3 mm. The area of the films is 100×45 mm.
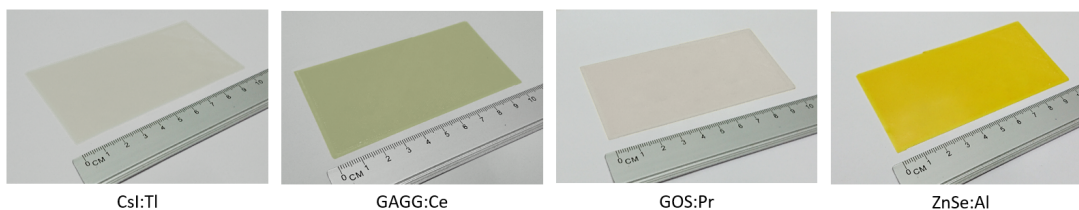

Figure 16. 3D printed samples for X-ray imaging.

As a reference, composite samples based on GOS:Pr (size of granules was 1–5 µm), size of $60 \times 40 \times 0.10$ mm was used. Organic polysiloxane matrix was prepared as a reference, as shown in [9]. The best results for 3D printed samples were obtained at a film thickness of 0.15 mm. Spatial resolution for these 3D printed films were from 3.15 line pairs per mm to 3.35 line pairs per mm (table 5). X-ray imaging screens of 3D printed films are shown in figure 17. The radiation resistance of 3D printed samples will be studied in further research.
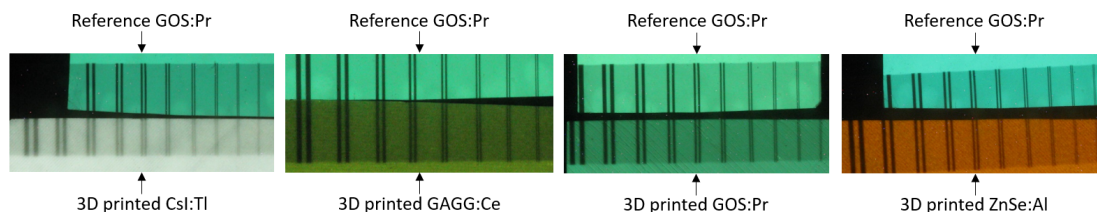

Figure 17. X-ray imaging screens of 3D printed films.

Table 5. Spatial resolution of 3D printed composite films 0.15 mm thick.

Scintillator	Reference GOS:Pr	ZnSe:Al	GOS:Pr	GAGG:Ce	CsI:Tl
Spatial resolution line pairs per mm	3.85	3.15	3.35	3.35	3.15

4 Conclusions

Using 3D printing, it is possible to manufacture large area detectors. There is no need for post-processing: the surface is ready for connection with the PMT or SiPM. It is cost effective due to the possibility of using the waste material from the production of single crystals.

The developed scintillators can be used for the registration of X-ray radiation and for the detection of alpha and beta particles. Moreover, the developed scintillators can be used in high-energy physics. For example, 3D printing technology will permit the easier development of finely segmented EM calorimeters.

Further development of 3D printing of scintillators can be directed to the creation of radiation hardness scintillators and the creation of combined detectors.

References

[1] *The 3D Printed Detector (3DET) project*, https://threedet.web.cern.ch.

[2] S. Berns, A. Boyarintsev, S. Hugon, U. Kose, D. Sgalaberna, A. De Roeck et al., *A novel polystyrene-based scintillator production process involving additive manufacturing*, 2020 *JINST* **15** 10 [arXiv:2011.09859].

[3] 3DET collaboration, *Additive manufacturing of fine-granularity optically-isolated plastic scintillator elements*, 2022 *JINST* **17** P10045 [arXiv:2202.10961].

[4] A. Blondel et al., *A fully active fine grained detector with three readout views*, 2018 *JINST* **13** P02006 [arXiv:1707.01785].

[5] C. Dujardin, E. Auffray, E. Bourret-Courchesne, P. Dorenbos, P. Lecoq, M. Nikl et al., *Needs, Trends, and Advances in Inorganic Scintillators*, *IEEE Trans. Nucl. Sci.* **65** (2018) 1977.

[6] E. Auffray, *Scintillation properties and radiation hardness of the Ce-doped, Codoped Ce, Mg garnet crystals and garnet crystal fibers development, LHCB upgrade calorimeter*, talk given at the *Upgrade Ib/II calorimeter meeting*, CERN, Geneva, Switzerland, 23 February 2018, https://indico.cern.ch/event/706303/contributions/2898330/attachments/1605966/2548030/GarnetpropertiesEauffray23022018.pdf.

[7] L. Martinazzoli, N. Kratochwil, S. Gundacker and E. Auffray, *Scintillation properties and timing performance of state-of-the-art $Gd_3Al_2Ga_3O_{12}$ single crystals*, *Nucl. Instrum. Meth. A* **1000** (2021) 165231.

[8] V.Y. Degoda, G.P. Podust, N.Y. Pavlova and M. Alizadeh, *Formation of color centers at X-ray irradiation of ZnSe single crystals*, *Radiat. Meas.* **131** (2020) 106232.

[9] I. Gerasymov, T. Nepokupnaya, A. Boyarintsev, O. Sidletskiy, D. Kurtsev, O. Voloshyna et al., *GAGG:ce composite scintillator for x-ray imaging*, *Opt. Mater.* **109** (2020) 110305.

[10] A. Boyarintsev, N. Galunov, I. Gerasymov, N. Karavaeva, A. Krech, L. Levchuk et al., *Radiation-resistant composite scintillators based on GSO and GPS grains*, *Nucl. Instrum. Meth. A* **841** (2017) 124.

[11] A.Y. Boyarintsev, N.Z. Galunov, I.V. Gerasymov, T.E. Gorbacheva, B.V. Grinyov, N.L. Karavaeva et al., *Radiation Resistance of Composite Scintillators*, *Probl. Atom. Sci. Technol.* (2019) 60.

[12] A. Krech, N. Galunov, A. Boyarintsev et al., *Radiation Resistance of Composite Scintillators Based on Grains of Oxide Single Crystals*, Acta Phys. Polon. A, **141** (2022) 426 [http://przyrbwn.icm.edu.pl/APP/PDF/141/app141z4p39.pdf].

[13] T.A. Nepokupnaya, A.Y. Boyarintsev, B.V. Grynyov, S.M. Galkin and A.V. Kolesnikov, *The ways of characteristics improvement for alpha-beta detectors on ZnSe based composite scintillators*, *Nucl. Instrum. Meth. A* **1014** (2021) 165704.

[14] https://www.fritsch-international.com/.

[15] https://noztek.com/.

[16] https://www.creatbot.com/.

[17] S.O. Tretyak and O.V. Popkova, *A measuring complex for control the uniformity of the light output of scintillators*, *Funct. Mater.* **25** (2018) 835.

[18] S.M. Galkin, I.A. Rybalka, I.A. Tupitsyna, V.S. Zvereva, and V.A. Litichevskiy, *The development of flexible scintillation panels based on chalcogenide and oxide phosphors for advanced x-ray scanners and tomographs*, *Sci. Innovation* **12** (2016) 37.

[19] S. Barsuk, *The Shashlik Electro-Magnetic Calorimeter for the LHCb Experiment*, Tech. Rep., LHCb-PROC-2004-006, CERN, Geneva (2004).

[20] http://www.isma.kharkov.ua/en/node/31.